Sparse Current Source Estimation for MEG Using Loose Orientation Constraints

Wei-Tang Chang,[1] Seppo P. Ahlfors,[2,3] and Fa-Hsuan Lin[1,2,4]*

[1]*Institute of Biomedical Engineering, National Taiwan University, Taipei, Taiwan*
[2]*Department of Radiology, Athinoula A. Martinos Center for Biomedical Imaging, Massachusetts General Hospital, Charlestown, Massachusetts*
[3]*Harvard-MIT Division of Health Sciences and Technology, Cambridge, Massachusetts*
[4]*Department of Biomedical Engineering and Computational Science, Aalto University School of Science, Espoo, Finland*

Abstract: Spatially focal source estimates for magnetoencephalography (MEG) and electroencephalography (EEG) data can be obtained by imposing a minimum ℓ^1-norm constraint on the distribution of the source currents. Anatomical information about the expected locations and orientations of the sources can be included in the source models. In particular, the sources can be assumed to be oriented perpendicular to the cortical surface. We introduce a minimum ℓ^1-norm estimation source modeling approach with loose orientation constraints (ℓ^1LOC), which integrates the estimation of the orientation, location, and strength of the source currents into a cost function to jointly model the residual error and the ℓ^1-norm of the source estimates. Evaluation with simulated MEG data indicated that the ℓ^1LOC method can provide low spatial dispersion, high localization accuracy, and high source detection rates. Application to somatosensory and auditory MEG data resulted in physiologically reasonable source distributions. The proposed ℓ^1LOC method appears useful for incorporating anatomical information about the source orientations into sparse source estimation of MEG data. *Hum Brain Mapp 34:2190–2201, 2013.*   © **2012 Wiley Periodicals, Inc.**

Key words: inverse problem; ℓ^1-norm; convex optimization; MEG; EEG; orientation constraint

INTRODUCTION

Magnetoencephalography (MEG) and electroencephalography (EEG) are techniques to noninvasively detect extracranial magnetic fields and scalp potentials elicited by electrical activity in the human brain. In distributed source modeling of MEG and EEG data, the amplitudes and orientations of a large number of current sources at predetermined locations are estimated [Baillet et al., 2001]. This is achieved by minimizing a cost function, which usually consists of two terms, one describing the modeling errors and the other a constraint on the source amplitudes. A popular method called the minimum-norm estimate (MNE) is based on a linear inverse operator that minimizes the ℓ^2-norm of the source amplitudes [Hämäläinen and Ilmoniemi, 1984].

The MNE tends to provide diffuse source estimates even when the true source currents are focal. One way to construct less diffuse source estimates is to impose a minimum ℓ^1-norm constraint on the source amplitudes [Matsuura and Okabe, 1995; Uutela et al., 1999].

A priori anatomical and physiological information about the locations and orientations of the sources can be incorporated into distributed source models. Specifically, the source currents can be assumed to be located at the cerebral cortex and oriented perpendicular to the cortical surface [Dale and Sereno, 1993]. An accurate orientation constraint can improve the MEG localization accuracy [Lin et al., 2006a; Robinson and Vrba, 1999]. However, a strict orientation constraint (SOC), which enforces the current dipoles to be exactly perpendicular to the local cortical surface, can lead to inaccurate source estimates if the source space is too sparse with respect to the curvature of the cortical surface. Source space subsampling is motivated by the limited spatial resolution intrinsic to MEG and by practical concerns of computational efficiency. The downside of such subsampling is that the simplified source geometry does not take into account the variation in the cortical surface orientation near each subsampled current source location. Therefore, the orientation of the source element at the location closest to the true activation does not necessarily match the orientation of the actual source. In this case, the largest current in the source estimate is likely to occur at a nearby location with a source orientation matching that of the true source. Moreover, inaccurate source estimates can also be caused by errors in the coregistration between MEG/EEG and MRI data. To alleviate these problems, a loose orientation constraint (LOC) on the source currents was introduced [Lin et al., 2006a]. Typically, the source space in distributed source models consists of current dipoles placed at fixed locations 3 to 10 mm apart from each other. With the LOC approach, it is possible to take into account the variability of the source orientations within a cortical patch around each selected source location by weighting the perpendicular and tangential source components differently.

Previously, LOC has been applied to minimum ℓ^1-norm estimation indirectly [Lin et al., 2006a], by first determining the source orientation using the ℓ^2-based MNE solution, as in the MCE method [Uutela et al., 1999], but computed with LOC. The minimum ℓ^1-norm constraint was used to determine the strength of this fixed-orientation source at each location [Lin et al., 2006a]. Here we call this previously presented method MCELOC. A potential problem with this approach is that incorrect source orientations from the MNE may result in mislocalization of the sources. In a related approach called VESTAL, MNE was also employed before applying the minimum ℓ^1-norm constraint, but instead of strictly constraining the source orientations, only the sign of each directional component was used [Huang et al., 2006]. However, the minimum ℓ^1-norm constraint tends to bias current estimates to be oriented along the x-, y-, or z-direction. Although this bias can be reduced by imposing different weights on the three orthogonal directions [Huang et al., 2006], ideally the source estimates should be invariant with respect to the choice of the local coordinate axes. One way to achieve this invariance is to subject the directional components to the minimum ℓ^2-norm constraint at each source location [Ding and He, 2008; Ou et al., 2009]. The source strengths and orientations of the minimum ℓ^1-norm solution can be determined directly using second-order cone programming (SOCP) [Mittelmann, 2003], without involving MNE. In a sense, the minimum ℓ^1-norm and minimum ℓ^2-norm constraints are applied at different spatial scales: locally the orientation of the estimated source current is allowed to vary freely, and globally a spatially sparse source distribution is preferred.

In the present study we propose to incorporate LOC into the joint minimum $\ell^1\ell^2$-norm method. With this approach, named ℓ^1LOC, a priori constraints on the relative weights on the source components can be imposed, without relying on the MNE to fix the orientations. Using simulated and real MEG data, we demonstrate that the ℓ^1LOC approach has the potential to improve the accuracy of localizing focal sources. In this article, we consider only MEG, but the principles are expected to be applicable to EEG as well.

METHODS

Forward Model

The relationship between the measured MEG signals and the underlying neuronal currents can be modeled as:

$$\mathbf{y}(t) = \mathbf{A}\,\mathbf{s}(t) + \mathbf{n}(t) \tag{1}$$

where $\mathbf{y}(t)$ is an m-dimensional vector containing the observed data in m sensors at time t, $\mathbf{A}$ is an m-by-$3n$ forward matrix, $\mathbf{s}(t)$ is a $3n$-dimensional vector representing the unknown current sources consisting of the x-, y-, and z-components of n current dipoles, and $\mathbf{n}(t)$ is additive noise. Usually $3n$ is much larger than m and thus the matrix $\mathbf{A}$ has more columns than rows. For convenience, we assume that Eq. (1) describes prewhitened data such that the data vector, the forward matrix, and the noise vector have been multiplied by $\mathbf{C}^{-1/2}$, where $\mathbf{C}$ is the estimated noise covariance matrix of the unwhitened data [Lin et al., 2006a]. The prewhitening process allows us to assume that the noise measurements on different sensors are spatially uncorrelated. We also assume that the forward matrix $\mathbf{A}$ is constructed such that the $(3i)^{\text{th}}$ column of $\mathbf{A}$ represents the signals in the MEG sensors that would be generated by a current dipole oriented normal to the cortical surface (local z-direction) at the ith source location. The $(3i-1)^{\text{th}}$ and $(3i-2)^{\text{th}}$ columns of $\mathbf{A}$ correspond to the signals generated by a unit dipole in the local x and y directions, respectively.

Minimum ℓ^1-Norm Estimates With Orientation Constraints

Source estimation refers to the problem of determining $\mathbf{s}(t)$ for given data $\mathbf{y}(t)$ and known forward matrix $\mathbf{A}$. In the present study we will only consider instantaneous source estimates; therefore, to simplify the notation, we leave out the explicit time dependence. The minimum ℓ^1-norm constraint [Lin et al., 2006a; Matsuura and Okabe, 1995; Uutela et al., 1999] can be written as

$$\arg \min_{\mathbf{s}} ||\mathbf{s}||_1 = \arg \min_{s} \sum_i (|s_{i,x}| + |s_{i,y}| + |s_{i,z}|),$$
$$\text{s.t.} \left\| \mathbf{y}_r - \mathbf{A}_r \mathbf{s} \right\|_2^2 \leq \varepsilon, \tag{2}$$

where $S_{i,x}$, $S_{i,y}$, and $S_{i,z}$ are the three local source components at location i. Here $\mathbf{y}_r = \mathbf{U}_r^T \mathbf{y}$ and $\mathbf{A}_r = \mathbf{U}_r^T \mathbf{A}$ are the regularized versions of the measurement data vector and the forward matrix, respectively, obtained with the help of a truncated singular value decomposition of $\mathbf{A} = \mathbf{U}\mathbf{\Lambda}\mathbf{V}^T$. The matrix $\mathbf{U}_r$ contains the first r columns of $\mathbf{U}$, corresponding to the r largest singular values of $\mathbf{A}$. The regularization by truncation helps to reduce sensitivity to noise, and the lower rank of the forward matrix reduces the computational load [Uutela et al., 1999]. The number of truncated singular vectors is selected to control the total lead field power [Lin et al., 2006a]. The parameter ε in Eq. (2) controls the consistency between the measured data and the values predicted from the estimated sources. In the MCE approach, ε was set to zero [Uutela et al., 1999]. However, one can choose ε such that the probability of $\|\mathbf{y}_r - \mathbf{A}_r\mathbf{s}\|_2^2 > \varepsilon$ is small [Ding and He, 2008]. Assuming Gaussian white noise with variance σ^2, we have $\|\mathbf{y}_r - \mathbf{A}_r\mathbf{s}\|_2^2/\sigma^2 \sim \chi_r^2$, where χ_r^2 is the Chi-square distribution with r degrees of freedom. In practice, ε can be selected such that the probability of the random variable $\|\mathbf{y}_r - \mathbf{A}_r\mathbf{s}\|_2^2$ ranging between $[0, \varepsilon]$ equals to a predefined value (such as 0.99).

The source estimates obtained using Eq. (2) tend to align along the coordinate axes at each source location [Huang et al., 2006]. A solution that is invariant with respect to the choice of the local coordinate axes is obtained by minimizing the ℓ^1-norm of a vector whose elements are the ℓ^2-norm of the estimated source current $\mathbf{s}_i$ at location i:

$$||\mathbf{s}_i||_2 = \left[s_{i,x}^2 + s_{i,y}^2 + s_{i,z}^2 \right]^{1/2}. \tag{3}$$

In the present study, we propose imposing a loose constraint on the orientation for each source by using a weighted ℓ^2-norm $\|\mathbf{W}_i\mathbf{s}_i\|_2$. We use the specific form

$$\mathbf{W}_i = \text{diag}[1/\sin\theta_i, 1/\sin\theta_i, 1] \tag{4}$$

for each location i [Lin et al., 2006a]. The orientation constraint parameter θ_i, ranging from $0°$ to $90°$, allows different relative proportions between the local perpendicular

$(z\text{-})$ and local tangential (x- and y-) components. In the practical implementation, we used

$$||\mathbf{W}_i\mathbf{s}_i||_2 = \left[(\frac{s_{i,x}}{\sin\theta_i + \delta})^2 + (\frac{s_{i,y}}{\sin\theta_i + \delta})^2 + (s_{i,z})^2 \right]^{1/2} \tag{5}$$

where the minimum positive floating-point value δ was included to avoid division by 0 in Eq. (4). When $\theta_i = 90°$, then $\mathbf{W}_i = \mathbf{I}$ (identity matrix), corresponding to the free orientation (FO) case. When $\theta_i = 0°$ only z-direction components are allowed and this is equal to the strict orientation constraint (SOC) case. The minimum ℓ^1-norm solution with $\theta_i = 90°$ and $\theta_i = 0°$ are called ℓ^1FO and ℓ^1SOC, respectively.

The weighting as specified in Eq. (4) will cause some bias between source locations with different θ_i, as the squared inverse of $\mathbf{W}_i$ can be interpreted to be the a priori source covariance matrix. To equalize the a priori source power, a normalization factor of $\sqrt{2\sin^2\theta_i + 1}$ could be applied. Since the effect of this adjustment is expected to be small (the factor ranging from 1 to $\sqrt{3}$), we did not implement it in our calculations. However, appropriate normalization is important when additional priors are included, such as depth weighting (or lead field normalization) [Lin et al., 2006b] or fMRI-based constraints.

With the loose orientation constraint, Eq. (2) is modified to be

$$\arg \min_{\mathbf{s}} \sum_i ||\mathbf{W}_i\mathbf{s}_i||_2,$$
$$\text{s.t.} \left\| \mathbf{y}_r(t) - \mathbf{A}_r\mathbf{s} \right\|_2^2 \leq \varepsilon. \tag{6}$$

Since the feasible set of $\|\mathbf{y}_r - \mathbf{A}_r\mathbf{s}\|_2^2 \leq \varepsilon$ is a convex set and $\sum \|\mathbf{W}_i\mathbf{s}_i\|_2$ is a convex function [Boyd, 2004], Eq. (6) can be solved by convex optimization techniques [Grant and Boyd, 2009]. Specifically, we used the following convex formulation of the optimization problem to solve $\mathbf{s}$ via an auxiliary variable $\mathbf{s}^{\ell 2}$:

$$\arg \min_{s,s^{\ell 2}} ||\mathbf{s}^{\ell 2}||_1$$
$$\text{s.t.} \left\| \mathbf{y}_r - \mathbf{A}_r\mathbf{s} \right\|_2^2 \leq \varepsilon, \text{ and} \tag{7a}$$

$$||\mathbf{W}_i\mathbf{s}_i||_2 \leq s_i^{\ell 2}, \forall i = 1, \ldots, n. \tag{7b}$$

When $\|\mathbf{s}^{\ell 2}\|_1$ has the minimum, the inequality constraint in Eq. (7b) is satisfied with the equality and $\|\mathbf{s}^{\ell 2}\|_1$ is reduced to the sum of $\|\mathbf{W}_i\mathbf{s}_i\|_2$ across all source locations. This is exactly the ℓ^1-norm of the vector, each element of which is the local ℓ^2-norm of the three weighted directional source components.

Variation of the Surface Normal Within Cortical Patches

Due to the spatial smoothness of MEG lead fields and for considerations of computational efficiency, distributed source

modeling approaches usually employ a spacing of 5 to 10 mm between neighboring dipoles in a discrete source space [Uutela et al., 1999]. Hence, the orientation of the source currents may vary considerably within a patch of curved cortical surface surrounding each dipole location. A cortical patch can be defined as the set of vertices in the original dense cortex triangulation sharing the same nearest subsampled dipole location [Lin et al., 2006a]. Within each cortical patch i, we computed the standard deviation σ_i^θ of the angle between the vertex normals $\mathbf{n}_k$ in the dense cortex triangulation and the surface normal $\mathbf{n}_i$ at the subsampled location:

$$\sigma_i^\theta = \sqrt{\frac{1}{N_i - 1}\sum_{k \in P_i}[\arccos(\mathbf{n}_k \cdot \mathbf{n}_i) - \frac{1}{N_i}\sum_{k \in P_i}\arccos(\mathbf{n}_k \cdot \mathbf{n}_i)]^2}$$
$$(1 \le i \le n) \tag{8}$$

where N_i denotes the number of vertices within the cortical patch P_i.

For the orientation constraint parameter θ_i in Eq. (5), we propose to use the values

$$\theta_i = a\sigma_i^\theta, \tag{9}$$

where a is to be optimized using simulations. However, since computing σ_i^θ for each source location is computationally demanding, we also examined the simpler case of setting θ_i to a constant value across the whole cortex.

Performance Measures

The performance of the inverse solutions was assessed with three metrics: spatial dispersion (SD) [Molins et al., 2008], distance of localization error (DLE) [Molins et al., 2008], and the area under a receiver operating characteristic (ROC) curve [Darvas et al., 2004].

The SD was defined as:

$$SD = \sqrt{\frac{\sum_{k=1}^{K}\sum_{i \in I_k}d_{ki}^2||\hat{s}_i||_2^2}{\sum_{i=1}^{n}||\hat{s}_i||_2^2}}, I_k = \left\{i\Big|k = \arg\min_k\{d_{ki}\}\right\}, \tag{10}$$
$$1 \le k \le K,$$

where $\hat{s}_i$ is the estimated source current at location i, d_{ki} denotes the distance between the kth true source and the ith source estimate, and $-K$ is the number of the underlying current sources. I_k is the set of source space indices for which the kth of true sources is the spatially closest. To avoid overriding contributions from source estimates with small values but large distances, only source estimates with magnitude exceeding 10% of the global maximum were taken into the calculation of I_k.

The DLE was defined as

$$DLE = \frac{1}{K_J}\sum_{k \in J}DLE_k, \quad J = \{k|I_k \notin \phi\},$$
$$DLE_k = \left\{d_{ki}\Big|i = \arg\max_{i'}\{||\hat{s}_{i'}||_2\}, i' \in I_k\right\}, \tag{11}$$

where K_J denotes the number of elements in J, which is the set including indices of the detected true sources. The DLE_k measures the distance between the kth true source and maximum source estimate in I_k and DLE is the average of DLE_k over the true source indices k.

A receiver-operating characteristic (ROC) curve is a graphical plot of the rate of true positive detection (TP) versus the rate of false-positive detection (FP) as its discrimination threshold varies. In our study, the discrimination threshold ranged from 0% to 100% of the maximum of source estimates. The FP and TP were defined as

$$FP = \frac{N_{fd}}{n - N_s} \text{ and } TP = \frac{N_d}{N_s}, \tag{12}$$

where N_d and N_{fd} are the number of detected true and false sources, respectively. The number of total estimated sources at a given threshold is $N_d + N_{fd}$ and the number of true sources is N_s. We calculated the area under the ROC curve ($0.5 \le area \le 1$) to quantify the performance of the inverse methods. The ideal performance corresponds to area = 1.

MATERIALS

Anatomical Information From High Resolution MRI

Structural MRI data were acquired on a 3T MRI scanner (Tim Trio, SIEMENS Medical Solutions, Erlangen, Germany) using a T1-weighted 3D MPRAGE sequence with following parameters: repetition time/echo time/inversion time [TR/TE/TI] = 2,530/3.49/1,100 ms, flip angle = 7 degrees, partition thickness = 1.33 mm, image matrix = 256 × 256, 128 partitions, and a field-of-view = 21 × 21 cm². We used the FreeSurfer software [Dale et al., 1999; Fischl et al., 1999] to perform segmentation and to build cortical surface meshes from the MRI data. These cortical surfaces were used to generate the source space in MEG sources analysis, to calculate the forward solution $\mathbf{A}$ with realistic anatomy, and to visualize the source localization results. The cortical surface was defined using the boundary between the gray and white matter. FreeSurfer generated triangulated surface models with 130,000 to 150,000 vertices per hemisphere, separated by approximately 1 mm from each other. The source space used for the MEG source estimation was created by subsampling the cortical vertices into a semiregular model with 1,026 dipole locations in each hemisphere; the average distance between any two neighboring source dipoles was 10 mm. The

coregistration between MEG and MRI coordinates was done by manually registering in the MPRAGE data three fiducial points and a set of points on the scalp whose locations were identified with a digitizer with respect to head position indicator coils used in the MEG sessions. The MEG forward solution was calculated using a single layer boundary element model (BEM) [Hämäläinen and Sarvas, 1989; Oostendorp and van Oosterom, 1989] based on the inner-skull surface created by the FreeSurfer.

Simulated MEG Data

Simulated MEG data were generated by assuming three simultaneously active focal sources at randomly selected locations within three cortical regions [one source per region: the left primary somatosensory cortex (SI), the left middle temporal gyrus (MTG), and the right inferior frontal gyrus (IFG)]. In additional simulations, we selected two sources at fixed locations at the SI and the secondary somatosensory cortex (SII) in the left hemisphere, corresponding to expected source locations in our somatosensory experiment.

The orientation of each source was varied randomly over repeated simulations, such that the average orientation equaled to the surface normal at that location, and the standard deviation of the orientation equaled to σ_i^θ. Gaussian noise was added to the simulated data with signal-to-noise power ratio (SNR) of 25. The SNR was defined as $\|\mathbf{As}\|_2^2 / m\sigma_n^2$, where σ_n^2 denotes the noise variance. The calculation was repeated 100 times.

To avoid the "inverse crime" of using identical forward solutions for generating simulated data and for computing the inverse estimates [Kaipio and Somersalo, 2005], which often leads to overly optimistic localization performance, we generated two forward solutions using different source space grids. Simulated data were generated with an average of 2.5 mm separation between sources, whereas the inverse solution was calculated with an average of 10 mm separation. Each source space was constructed independently; the one with an average of 10 mm separation was not a subset of the source space with an average of 2.5 mm separation.

Errors in the coregistration between MEG/EEG and MRI data are one potential cause of inaccuracy in SOC source estimates. To examine the effect of coregistration error, we generated simulated MEG data with the original forward matrix but calculated the inverse solution with a forward matrix obtained by randomly shifting the head position by 1, 2, 4, or 8 mm, yielding an inaccurate coordinate transformation and thus an incorrect forward matrix.

MEG Experiments

To test the method with empirical data, we performed somatosensory and auditory MEG experiments. Six healthy, right-handed subjects (four males, two females; average age = 27 years) participated, with the approval of the Institutional Review Board (IRB) of National Taiwan University. Before the experiments, an informed consent was obtained from each subject. A 306-channel MEG system (VectorView, Elekta-Neuromag, Helsinki, Finland) was used to record the neuromagnetic responses.

In the somatosensory study, the right median nerve was stimulated at the wrist with current pulses of 0.2 ms duration (Konstant-Strom Stimulator, Lucius & Baer, Geretsried, Germany). The amplitude of the stimulation was adjusted to clearly observe thumb adduction. The interstimulus interval was 5 s. We collected 180 responses in each subject. In the auditory experiment, 1 kHz pure tones were presented to the right ear. The interstimulus interval was 4 s. About 100 responses were averaged. The measurement bandwidth was 0.03 to 260 Hz and the data were digitized at 1004 Hz.

Implementation

To perform convex optimization, we employed the CVX software package [Grant and Boyd, 2009] in MATLAB (Mathworks, Natick, MA). This method converged within 100 iterations in all our simulations and experiments. The number of rows for truncated SVD-regularized forward matrix r was selected in order to include 99% of the total lead field power. For the six subjects in the present study, the truncation parameter r [Eq. (2)] ranged from 46 to 77 for the full $\mathbf{A}$ matrix (FO case). The r value for the reduced $\mathbf{A}$ matrix for the SOC case (containing only every third column of the full forward matrix) were similar, with only 1 to 4 additional SVD components being truncated. Furthermore, a minor change in r will be partly compensated by an adjustment of the value of ε in Eq. (6). Since small changes in r were expected to affect the solutions only little, we used the same FO-based r value for an individual subject when computing the inverse solutions with varying levels of orientation constraints. For $r = 77$ (the rank of the regularized forward matrix) and $n = 2{,}052$ (the number of source locations) in our study, calculation of the ℓ^1LOC estimate for one time point of MEG data took about 68 s on a standard PC (1.6 GHz CPU and 2G bytes RAM).

For visualization, the source estimates were normalized by the maximum value in each map. The magnitude of the estimated activity for individual source elements may differ substantially due to differences in the spatial spread of the inverse solutions. For example, a factor of 2 difference in the magnitude could result from assigning all estimated source activity to a single source element versus spreading the activity to two neighboring locations. Therefore, the normalization helps to better illustrate the localization precision of the different approaches.

RESULTS

Variability in Source Orientations

We first examined how much variability in the source orientation is expected within the local patches of curved cortex around the discrete locations used for the MEG
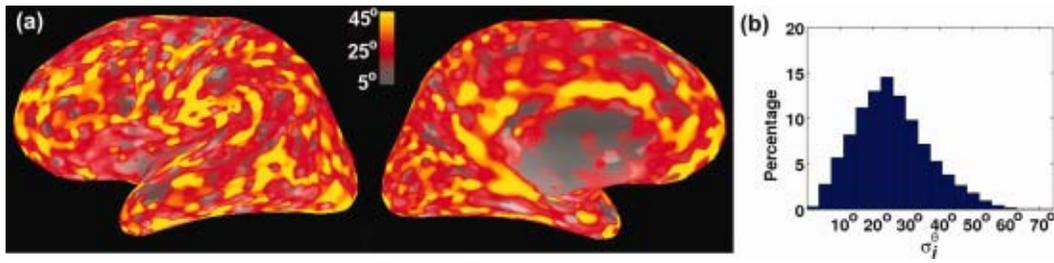
Figure 1.

Distribution of the standard deviation σ_i^θ of the angle between the vertex normals within the cortical patches surrounding discrete source locations. (**a**) The spatial distribution of σ_i^θ for one subject (S1), shown on the lateral and medial view of an inflated reconstruction of the left cerebral cortex. The spacing between neighboring source locations was 10 mm; the total number of source locations was around 3,500. (**b**) A histogram of the σ_i^θ values in six subjects. [Color figure can be viewed in the online issue, which is available at wileyonlinelibrary.com.]

source modeling. An example of the spatial distribution of σ_i^θ is shown in Figure 1a. Combined data from six subjects indicated that 25%, 50%, 75%, and 95% of the orientation deviations of the vertex normals were less than 18°, 25°, 32°, and 45°, respectively (Fig. 1b).

Simulations

The sensitivity of the ℓ^1LOC method to the choice of the orientation constraint parameter θ_i was evaluated using three simulated sources randomly selected from the vicin-ity of the left SI, left MTG, and right IFG areas (see inset in the top left panel in Fig. 2a). Performance metrics for the spatially varying case where $\theta_i = a\sigma_i^\theta$ are shown in Figure 2a. The error measures SD and DLE were smallest when $a = 1.5$. The area under the ROC curve for $\theta_i = 0.5\sigma_i^\theta$, σ_i^θ, $1.5\sigma_i^\theta$, $2\sigma_i^\theta$ was 0.96, 0.98, 0.99, and 0.99, respectively. The performance with $\theta_i = 1.5\sigma_i^\theta$ was statistically significantly better than the performance with $\theta_i = 0.5\sigma_i^\theta$ and $\theta_i = \sigma_i^\theta$ in terms of SD and DLE ($P < 0.01$). However, the difference between the performance with $\theta_i = 1.5\sigma_i^\theta$ and $\theta_i = 2\sigma_i^\theta$ was not significant in any of the three
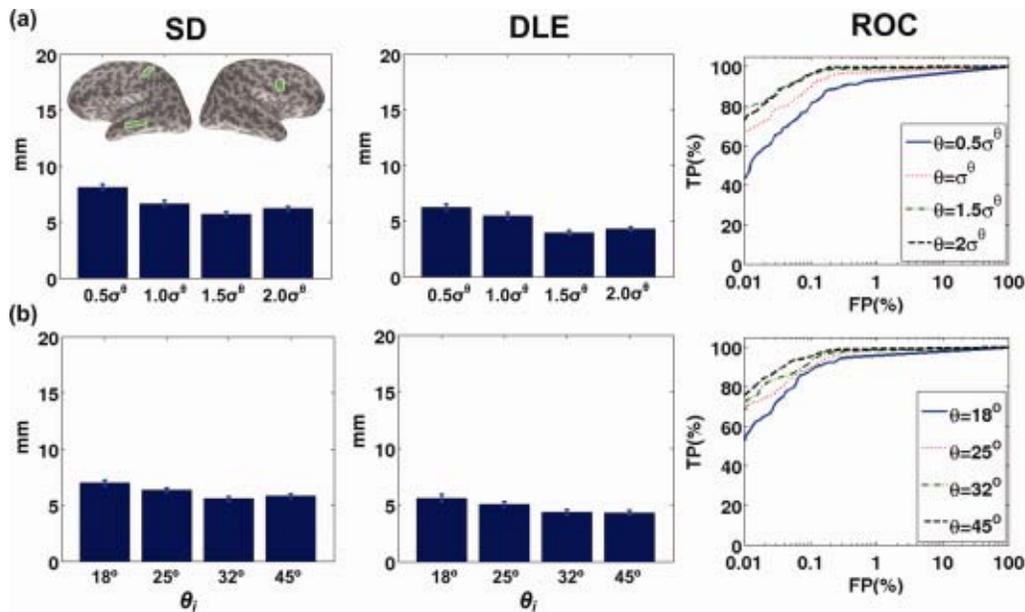

Figure 2.

Performance metrics (SD, DLE, and ROC) for ℓ^1LOC estimates for simulated MEG data, as a function of different values of the loose orientation constraint parameter θ_i. Three current dipole sources were randomly selected, one from each of the green regions shown in the inset. The standard deviation of the orientation of the simulated dipoles was σ_i^θ. The parameter θ_i was either (**a**) spatially varying, being proportional to σ_i^θ, or (**b**) spatially uniform, having a constant value for each source location. [Color figure can be viewed in the online issue, which is available at wileyonlinelibrary.com.]
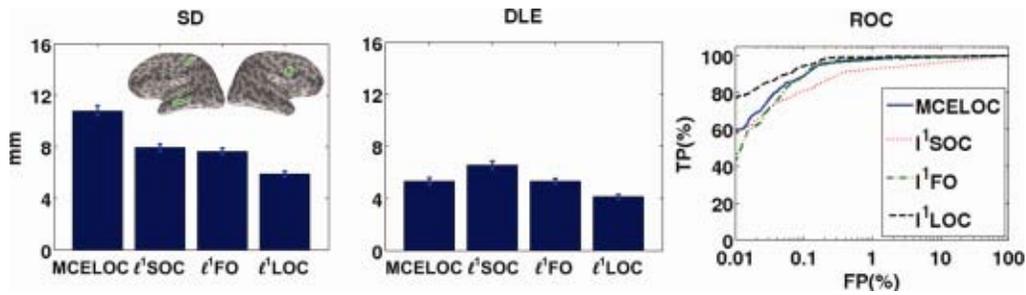
Figure 3.

Performance metrics SD, DLE, and ROC for the four different minimum ℓ^1-norm solutions: MCELOC, ℓ^1SOC, ℓ^1FO, and ℓ^1LOC. The locations of three true current sources were randomly selected from each of the three regions shown as green patches in the inflated cortical map. [Color figure can be viewed in the online issue, which is available at wileyonlinelibrary.com.]

performance measures ($P > 0.1$). Figure 2b shows the performance metrics when constant values of θ_i were used across the source locations. The performance with $\theta_i = 32°$ was better than with $\theta_i = 18°$ and $\theta_i = 25°$ in terms of SD and DLE ($P < 0.05$). However, the performance with $\theta_i = 32°$ was not significantly better than with $\theta_i = 45°$ in any of the three performance measures ($P > 0.4$). The area

under the ROC curve for $\theta_i = 18°$, $25°$, $32°$, and $45°$ were 0.98, 0.99, 0.99, and 0.99, respectively. Moreover, when comparing the performance with $\theta_i = 1.5\sigma_i^\theta$ versus $\theta_i = 32°$, no statistically significant differences were observed ($P = 0.66$ for SD, $P = 0.16$ for DLE, and $P = 0.46$ for the area under ROC). In the rest of this study, we used $\theta_i = 1.5\sigma_i^\theta$ unless otherwise noted.
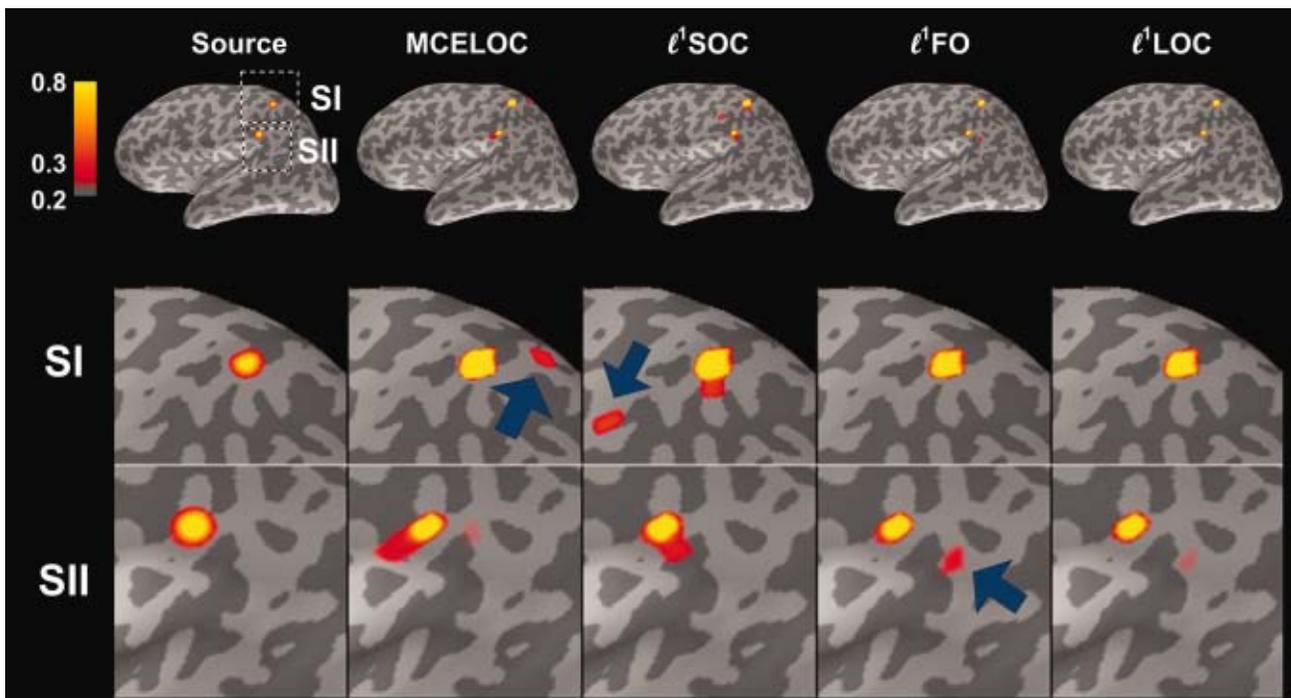

Figure 4.

Examples of minimum ℓ^1-norm source estimates for simulated MEG data, obtained with the MCELOC, ℓ^1SOC, ℓ^1FO, and ℓ^1LOC approaches. The true sources (left column) consisted of two focal sources corresponding to the somatosensory areas SI and SII in the left hemisphere. The estimates were normalized by dividing by the maximum value in each map. The activation strength is shown color-coded on an inflated cortical surface; dark and light gray denote sulcal and gyral regions, respectively. The dashed box indicates the region enlarged for better visualization. The blue arrows denote false-positive locations. [Color figure can be viewed in the online issue, which is available at wileyonlinelibrary.com.]
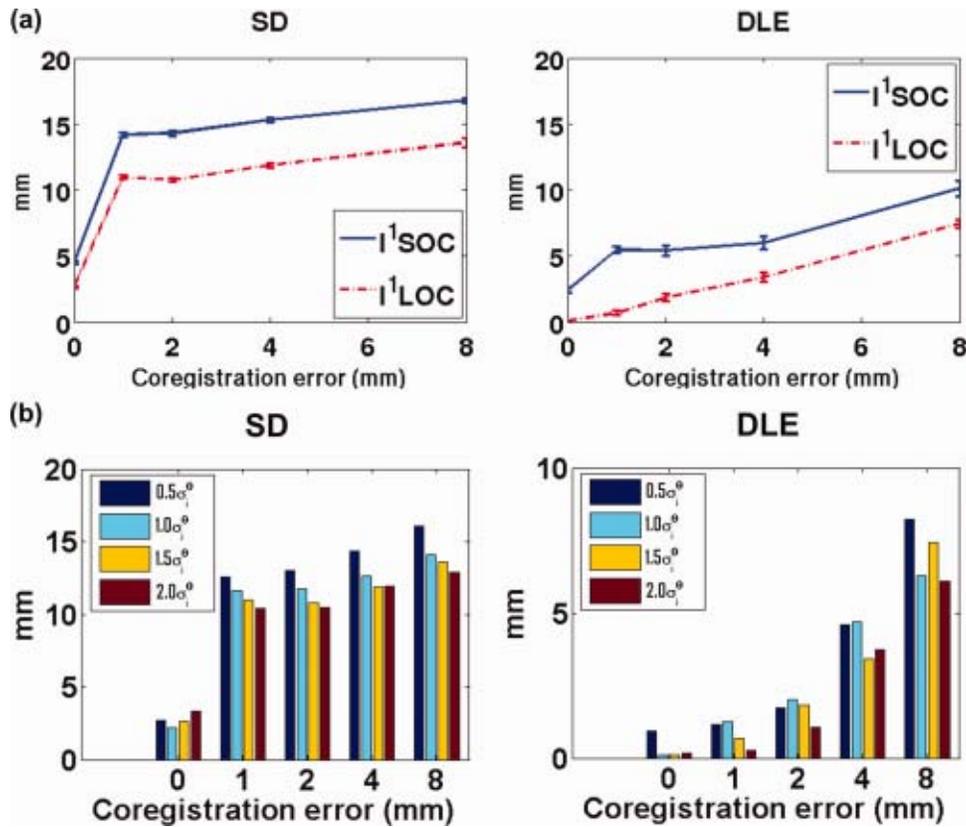
Figure 5.

Effect of coregistration error on the performance measures SD and DLE. The source estimates were calculated using an incorrect forward solution caused by a shift in the head position. **(a)** Comparison of the ℓ^1SOC and ℓ^1LOC source estimates. **(b)** Performance of the ℓ^1LOC method using different values of the loose orientation constraint $\theta_i = a\sigma_i^\theta$. [Color figure can be viewed in the online issue, which is available at wileyonlinelibrary.com.]

Performance metrics for simulated MEG data using four different source estimates subjected to the minimum ℓ^1-norm constraint are shown in Figure 3. The error measures SD and DLE were smaller for ℓ^1LOC than for MCE-LOC, ℓ^1SOC, and ℓ^1FO. The areas under the ROC curve for MCELOC, ℓ^1SOC, ℓ^1FO, and ℓ^1LOC were 1.00, 0.96, 0.99, and 1.00, respectively. The ℓ^1LOC outperformed the other methods in almost all the performance metrics. Compared with ℓ^1LOC, the SD and DLE values were significantly different for MCELOC, ℓ^1SOC, and ℓ^1FO ($P < 0.0001$ in all cases). Although the areas under ROC for MCELOC and ℓ^1FO were not significantly different from that for ℓ^1LOC ($P = 0.72$ for MCELOC and $P = 0.29$ for ℓ^1FO), the area under ROC for ℓ^1LOC was significantly larger than that for ℓ^1SOC ($P = 3.71 \times 10^{-5}$). In general, ℓ^1LOC provided higher estimation accuracy compared with the other approaches.

Figure 4 illustrates an example of the different source estimates when two simulated sources were assumed in SI and SII in the left hemisphere. In this particular case, the maps of the MCELOC, ℓ^1SOC, and ℓ^1FO solutions showed false-positive activity (indicated by blue arrows in Fig. 4)

in addition to the correct location. The ℓ^1LOC solution showed only minimal false-positive activation.

The effect of coregistration error on the performance metrics SD and DLE are shown in Figure 5a. In this simulation, two focal current sources were assumed at the left SI and SII. The ℓ^1LOC solution consistently outperformed the ℓ^1SOC solutions in the presence of coregistration error. We also examined the effect of the scaling factor a for σ_i^θ in Eq. (9), with different coregistration errors (Fig. 5b). The differences in the performance measures were small, suggesting that the choice of $\theta_i = 1.5\sigma_i^\theta$ is suitable even in the presence of coregistration errors.

Somatosensory and Auditory MEG Experiments

We applied the minimum ℓ^1-norm estimation methods with different orientation constraints to localize the neuronal current sources in the somatosensory and auditory experiments. Figure 6 shows source estimates for the somatosensory data of one subject using ℓ^1SOC, ℓ^1FO,
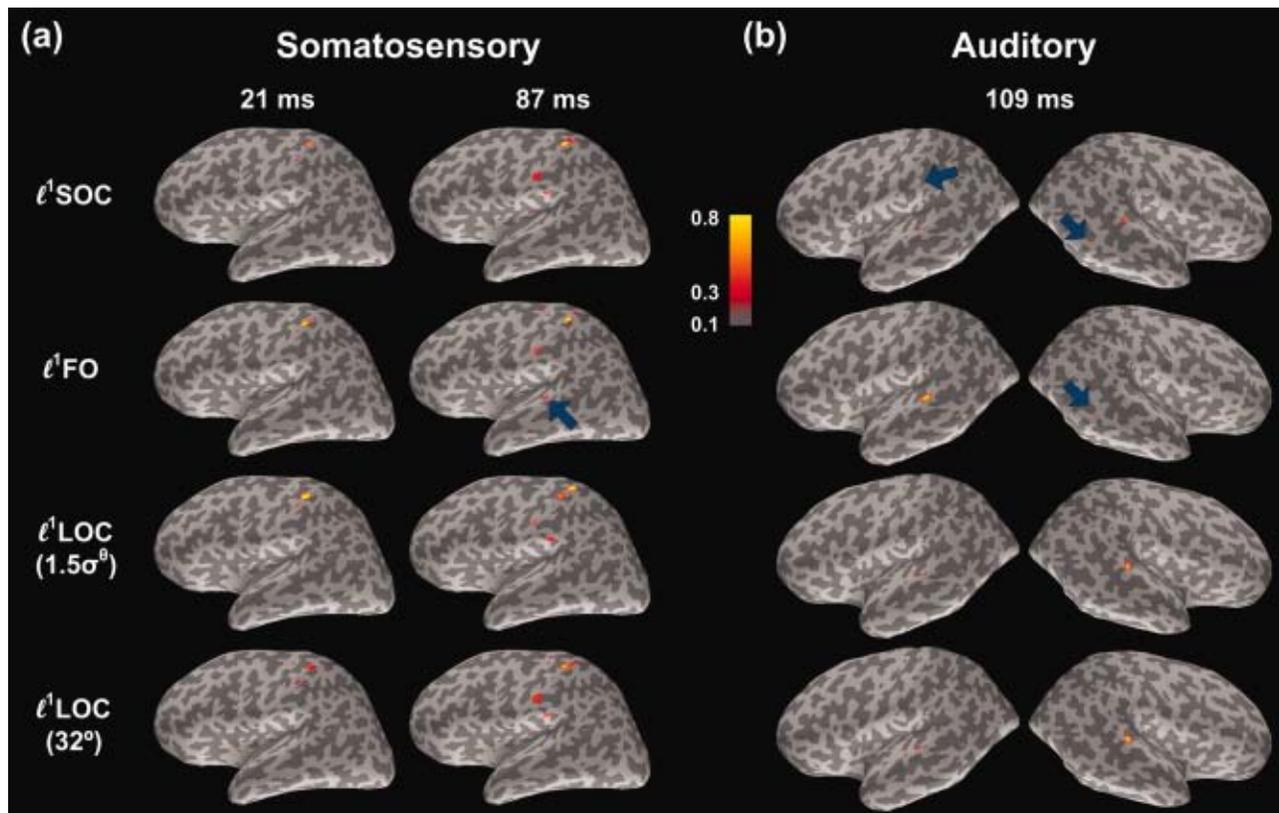
Figure 6.

Source estimates for somatosensory and auditory MEG data. Four different minimum ℓ^1-norm estimates are shown: ℓ^1SOC, ℓ^1FO, ℓ^1LOC with $\theta_i = 1.5\sigma_i^\theta$, and ℓ^1LOC with $\theta_i = 32°$. **(a)** Somatosensory evoked responses in the left hemisphere at two latencies, 21 and 87 ms after the right median nerve stimulation in one subject (S1). **(b)** Auditory evoked responses in the left and right hemispheres at 109 ms after tone stimulus onset (subject S4). The source strength was normalized to be between 0 and 1 for each map. Blue arrows indicate physiologically unlikely source locations. [Color figure can be viewed in the online issue, which is available at wileyonlinelibrary.com.]

ℓ^1LOC with $\theta_i = 1.5\sigma_i^\theta$, and ℓ^1LOC with $\theta_i = 32°$. All methods localized the early somatosensory response at about 21 ms latency into the posterior wall of the central sulcus, corresponding to the primary somatosensory cortex SI, and a later response, here shown at 87 ms, to the region of the secondary somatosensory cortex SII in the Sylvian fissure (Fig. 6a). These locations are consistent with those found in previous MEG studies [Hari and Forss, 1999]. The ℓ^1FO solution suggested activity also in the superior temporal gyrus (blue arrow in Fig. 6a); however, this location is unlikely to be activated in the median nerve stimulation experiment.

Figure 6b shows an example of the source estimates for the auditory data in one subject. All the different estimates showed bilateral activity at primary auditory cortices in the superior temporal gyrus, as expected for the N100m response [Tuomisto, et al. 1983]. The ℓ^1SOC and ℓ^1FO solutions showed physiologically unlikely activations at the right middle temporal gyrus and left inferior parietal lobe. The ℓ^1LOC solutions, both with the spatially varying LOC

parameter $\theta_i = 1.5\sigma_i^\theta$ and with the constant value $\theta_i = 32°$, showed little if any activation at these presumably incorrect locations.

The stability of ℓ^1LOC source estimates across subjects is illustrated in Figure 7. Consistent with previous literature [Hämäläinen et al., 1993; Hari and Forss, 1999], the ℓ^1LOC estimates suggested strong contralateral activation in SI at 35 ms for the somatosensory data, and in the primary auditory cortex at 86 ms for the auditory data in all three subjects studied in each experiment. In one of the subjects, the ℓ^1LOC estimates suggested inferior parietal activity, which is considered physiologically unlikely in the auditory experiment.

DISCUSSION

We refined sparse MEG source estimates by incorporating loose orientation constraints directly into the cost function. In simulations, the proposed ℓ^1LOC yielded source
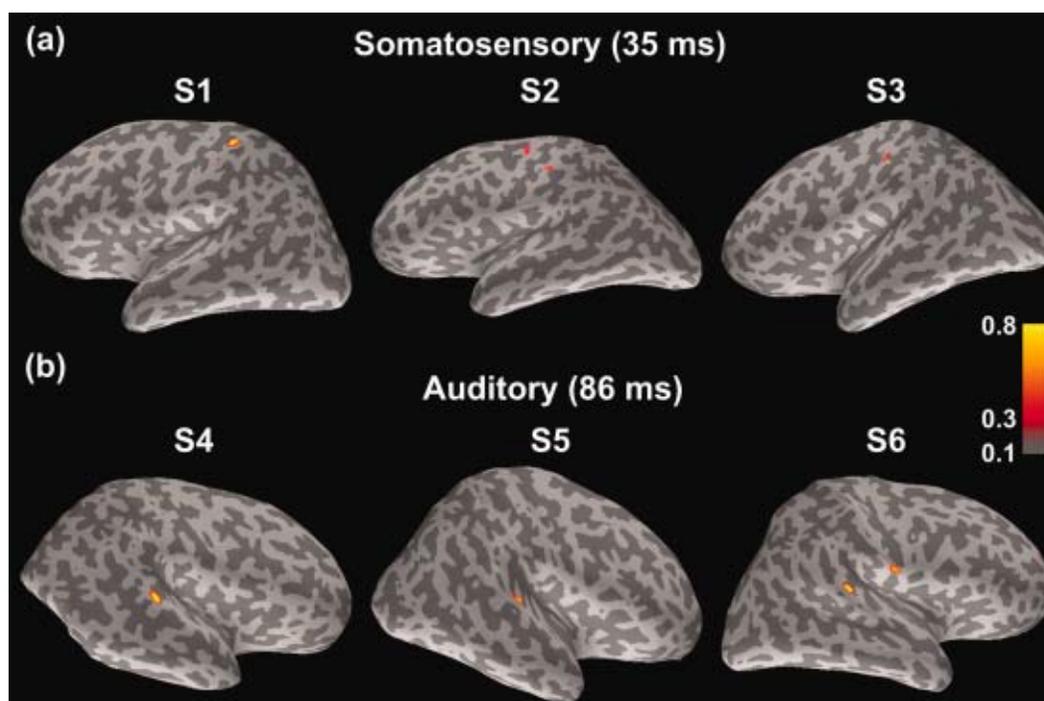
Figure 7.

Experimental results using ℓ^1LOC in different subjects. Maps of source estimates are shown (**a**) at 35 ms after the somatosensory stimulus onset and (**b**) at 86 ms after the auditory stimulus onset. S1 to S6 indicate different subjects. The estimates were normalized by dividing by the maximum value in each map. [Color figure can be viewed in the online issue, which is available at wileyonlinelibrary.com.]

estimates with low spatial dispersion, high localization accuracy, and high source detection rates. The average spatial dispersion and localization error of ℓ^1LOC were less than 10 mm, which was the average distance between two adjacent sources in our study. With real MEG data, the ℓ^1LOC solutions demonstrated physiologically reasonable source distributions for somatosensory and auditory evoked responses.

The importance of taking into account information about the source orientations has been noted for distributed source estimates [Lin et al., 2006a] as well as for beamformer spatial filtering techniques [Robinson and Vrba, 1999; Taniguchi et al., 2000]. In the present study, orientation constraints were integrated with the minimum ℓ^1-norm condition for distributed sources. The proposed ℓ^1LOC approach adjusts the source orientation automatically and adaptively in the convex optimization procedure. Hence, in contrast to MCELOC, the ℓ^1LOC approach avoids the potential inaccuracy caused by propagation of erroneous source orientations estimated by an initial calculation of an MNE solution.

The loose orientation constraint parameter θ_i can be set variably or uniformly across the brain. In our simulations, ℓ^1LOC with a spatially varied $\theta_i = 1.5\sigma_i^\theta$ and with a spatially uniform $\theta_i = 32°$ performed almost equally well. The use of a constant θ_i will save the users of ℓ^1LOC from the additional effort of acquiring a priori knowledge of the orientation variance.

Accurate estimation of sources on the opposite sides of a sulcus or a gyrus is challenging for any MEG and EEG source modeling approach. For example, in Figure 6b, the ℓ^1LOC method had difficulty to differentiate activities across the Sylvian fissure. One way to alleviate this problem is to explicitly minimize the difference between neighboring sources. Such technique has been implemented by integrating the ℓ^1-norm of the source estimates and the ℓ^1-norm of the Laplacian-transformed source estimates into the cost function [Chang et al., 2010]. Employing a Laplacian matrix in the cost function penalizes the spatial difference between the adjacent current sources on the cortical surface, and therefore suppresses physiologically atypical, spatially disconnected activations in opposite banks of a sulcus.

Although we only analyzed MEG data in the present study, in principle, the ℓ^1LOC method is applicable also to EEG source estimation. Some differences between MEG and EEG, however, may be expected in the interaction of the orientation constraint and the localization error, because MEG, but not EEG, is insensitive to one of the source components (i.e., radial orientation with respect to the skull) at most locations in the brain [Ahlfors et al., 2010].

In the present implementation, it took about one minute to compute the ℓ^1LOC estimate for one time instant of MEG data. The computation of a time sequence of the ℓ^1LOC estimates, like any approach that is applied independently to each time point, can be accelerated by parallel implementations [Nakata et al., 2006]. In contrast, methods like the $\ell^1\ell^2$-norm regularizer that uses temporal basis functions to ensure the temporal continuity of inverse solutions [Ou et al., 2009] cannot be easily parallelized.

A possible future enhancement of the ℓ^1LOC method is to develop measures of statistical inference, analogous to the dynamic statistical parametric mapping (dSPM) for the MNE [Dale et al., 2000]. In contrast to dSPM, statistical inference for ℓ^1LOC cannot be obtained analytically. However, the minimum ℓ^1-norm constraint implicitly assumes that the null distribution of current sources follows an exponential distribution [Uutela et al., 1999]. Hence, the parametric statistical inference of ℓ^1LOC can be derived using estimated parameters such as mean and standard deviation of the null distribution using procedures described by Pantazis et al. [2005].

CONCLUSIONS

We proposed ℓ^1LOC to estimate the orientation of current source automatically during sparse inverse modeling. The cost function explicitly penalizing the ℓ^1-norm of the sources tend to result in focal source estimates. The ℓ^1LOC estimates are spatiotemporally stable because the optimization problem includes a tolerance in the modeling residual error. As demonstrated by simulations and in vivo MEG data, ℓ^1LOC has the capability to provide accurate source localization and to enhance the spatial resolution by reducing spatial dispersion. In summary, we consider the ℓ^1LOC a useful method for integrating anatomical information into sparse source estimation.

ACKNOWLEDGMENTS

The authors are grateful for access to the MEG imaging resources at the Veteran General Hospital, Taipei, Taiwan, and the MRI resources at the National Yang-Ming University and National Taiwan University Hospital, Taipei, Taiwan. The authors also thank Chih-Che Chou for technical support.

REFERENCES

Ahlfors SP, Han J, Belliveau JW, Hämäläinen MS (2010): Sensitivity of MEG and EEG to source orientation. Brain Topogr 23:227–232.

Baillet S, Mosher J, Leahy R (2001): Electromagnetic brain mapping. IEEE Signal Process Magn 18:14–30.

Boyd S, Vandenberghe L (2004): Convex Optimization, Cambridge U.K., Cambridge University Press.

Chang WT, Nummenmaa A, Hsieh JC, Lin FH (2010): Spatially sparse source cluster modeling by compressive neuromagnetic tomography. Neuroimage 53:146–160.

Dale AM, Fischl B, Sereno MI (1999): Cortical surface-based analysis. I. Segmentation and surface reconstruction. Neuroimage 9:179–194.

Dale AM, Liu AK, Fischl BR, Buckner RL, Belliveau JW, Lewine JD, Halgren E (2000): Dynamic statistical parametric mapping: Combining fMRI and MEG for high-resolution imaging of cortical activity. Neuron 26:55–67.

Dale AM, Sereno MI (1993): Improved localization of cortical activity by combining eeg and meg with mri cortical surface reconstruction—A linear-approach. J Cogn Neurosci 5:162–176.

Darvas F, Pantazis D, Kucukaltun-Yildirim E, Leahy RM (2004): Mapping human brain function with MEG and EEG: Methods and validation. Neuroimage 23(Suppl 1):S289–S299.

Ding L, He B (2008): Sparse source imaging in electroencephalography with accurate field modeling. Hum Brain Mapp 29:1053–1067.

Fischl B, Sereno MI, Dale AM (1999): Cortical surface-based analysis. II: Inflation, flattening, and a surface-based coordinate system. Neuroimage 9:195–207.

Grant M, Boyd S (2009): CVX. Stephen Boyd, p. Matlab Software for Disciplined Convex Programming (wed page and software). Available at: http://standford.edu/~boyd/cvx. Accessed on Feb 17 2012.

Hämäläinen M, Hari R, Ilmoniemi RJ, Knuutila J, Lounasmaa OV (1993): Magnetoencephalography—Theory, instrumentation, and applications to noninvasive studies of the working human brain. Rev Mod Phys 65:413–497.

Hämäläinen M, Ilmoniemi R (1984): Interpreting Measured Magnetic Fields of the Brain: Estimates of Curent Distributions. Helsinki, Finland: Helsinki University of Technology.

Hämäläinen MS, Sarvas J (1989): Realistic conductivity geometry model of the human head for interpretation of neuromagnetic data. IEEE Trans Biomed Eng 36:165–171.

Hari R, Forss N (1999): Magnetoencephalography in the study of human somatosensory cortical processing. Philos Trans R Soc Lond B Biol Sci 354:1145–1154.

Huang MX, Dale AM, Song T, Halgren E, Harrington DL, Podgorny I, Canive JM, Lewis S, Lee RR (2006): Vector-based spatial-temporal minimum L1-norm solution for MEG. Neuroimage 31:1025–1037.

Kaipio J, Somersalo E (2005): Statistical and Computational Inverse Problems. New York: Springer.

Lin FH, Belliveau JW, Dale AM, Hämäläinen MS (2006a): Distributed current estimates using cortical orientation constraints. Hum Brain Mapp 27:1–13.

Lin FH, Witzel T, Ahlfors SP, Stufflebeam SM, Belliveau JW, Hämäläinen MS (2006b): Assessing and improving the spatial accuracy in MEG source localization by depth-weighted minimum-norm estimates. Neuroimage 31:160–171.

Matsuura K, Okabe Y (1995): Selective minimum-norm solution of the biomagnetic inverse problem. IEEE Trans Biomed Eng 42:608–615.

Mittelmann HD (2003): An independent benchmarking of SDP and SOCP solvers. Math Programming 95:407–430.

Molins A, Stufflebeam SM, Brown EN, Hämäläinen MS (2008): Quantification of the benefit from integrating MEG and EEG data in minimum l2-norm estimation. Neuroimage 42:1069–1077.

Nakata K, Yamashita M, Fujisawa K, Kojima M (2006): A parallel primal-dual interior-point method for semidefinite programs using positive definite matrix completion. Parallel Comput 32:24–43.

Oostendorp TF, van Oosterom A (1989): Source parameter estimation in inhomogeneous volume conductors of arbitrary shape. IEEE Trans Biomed Eng 36:382–391.

Ou W, Hämäläinen MS, Golland P (2009): A distributed spatio-temporal EEG/MEG inverse solver. Neuroimage 44:932–946.

Pantazis D, Nichols TE, Baillet S, Leahy RM (2005): A comparison of random field theory and permutation methods for the statistical analysis of MEG data. Neuroimage 25:383–394.

Robinson SE, Vrba J (1999): Functional neuroimaging by synthetic aperture magnetometry (SAM). In: Yoshimoto T, Kotani M, Kuriki S, Karibe H, Nakasato N, editors. Recent Advances in Biomagnetism. Sendai: Tohoku University Press. pp 302–305.

Taniguchi M, Kato A, Fujita N, Hirata M, Tanaka H, Kihara T, Ninomiya H, Hirabuki N, Nakamura H, Robinson SE, Cheyne D, Yoshimine T (2000): Movement-related desynchronization of the cerebral cortex studied with spatially filtered magneto-encephalography. Neuroimage 12:298–306.

Uutela K, Hämäläinen M, Somersalo E (1999): Visualization of magnetoencephalographic data using minimum current estimates. Neuroimage 10:173–180.